Cell

Drosophila Genome-wide Obesity Screen Reveals Hedgehog as a Determinant of Brown versus White Adipose Cell Fate

J. Andrew Pospisilik,[1,12,13] Daniel Schramek,[1,12] Harald Schnidar,[2] Shane J.F. Cronin,[1] Nadine T. Nehme,[3] Xiaoyun Zhang,[4] Claude Knauf,[5] Patrice D. Cani,[6] Karin Aumayr,[1] Jelena Todoric,[9] Martina Bayer,[9] Arvand Haschemi,[9] Vijitha Puviindran,[4] Krisztina Tar,[9] Michael Orthofer,[1] G. Gregory Neely,[1] Georg Dietzl,[7] Armen Manoukian,[8] Martin Funovics,[10] Gerhard Prager,[11] Oswald Wagner,[9] Dominique Ferrandon,[3] Fritz Aberger,[2] Chi-chung Hui,[4] Harald Esterbauer,[9,*] and Josef M. Penninger[1,*]

[1]Institute of Molecular Biotechnology of the Austrian Academy of Science, Dr. Bohrgasse 3, A 1030 Vienna, Austria
[2]Department of Molecular Biology, University of Salzburg, Hellbrunnerstrasse 34, A-5020 Salzburg, Austria
[3]Equipe Fondation Recherche Médicale, UPR 9022 du CNRS, Université de Strasbourg, Institut de Biologie Moléculaire et Cellulaire du CNRS,15 rue René Descartes F67084 Strasbourg, France
[4]Program in Developmental & Stem Cell Biology, The Hospital for Sick Children, and Department of Molecular Genetics, University of Toronto, Toronto, Ontario M5S 1A8, Canada
[5]INSERM U858, Team 3, Institut de Medecine Moleculaire de Rangueil, Paul Sabatier University, Bat. L4, IFR150, CHU Rangueil, BP 84225, 31432 Toulouse Cedex 4, France
[6]Université catholique de Louvain, LDRI, Unit PMNT-73/69, Av. E. Mounier, 73/69 B-1200 Brussels, Belgium
[7]Howard Hughes Medical Institute, Stanford University, 318 Campus Drive, Stanford, CA 94305, USA
[8]Ontario Cancer Institute/Princess Margaret Hospital, 610 University Avenue, Toronto, Ontario M5G 2M9, Canada
[9]Department of Medical and Chemical Laboratory Diagnostics
[10]Department of Radiology
[11]Department of Surgery
Medical University Vienna, Waehringer Guertel 18-20, A-1090 Vienna, Austria
[12]These authors contributed equally to this work
[13]Present address: Max Planck Institute of Immunobiology, Stübeweg 51, D-79108 Freiburg, Germany
*Correspondence: harald.esterbauer@meduniwien.ac.at (H.E.), josef.penninger@imba.oeaw.ac.at (J.M.P.)
DOI 10.1016/j.cell.2009.12.027

SUMMARY

Over 1 billion people are estimated to be overweight, placing them at risk for diabetes, cardiovascular disease, and cancer. We performed a systems-level genetic dissection of adiposity regulation using genome-wide RNAi screening in adult *Drosophila*. As a follow-up, the resulting ~500 candidate obesity genes were functionally classified using muscle-, oenocyte-, fat-body-, and neuronal-specific knockdown in vivo and revealed hedgehog signaling as the top-scoring fat-body-specific pathway. To extrapolate these findings into mammals, we generated fat-specific hedgehog-activation mutant mice. Intriguingly, these mice displayed near total loss of white, but not brown, fat compartments. Mechanistically, activation of hedgehog signaling irreversibly blocked differentiation of white adipocytes through direct, coordinate modulation of early adipogenic factors. These findings identify a role for hedgehog signaling in white/brown adipocyte determination and link in vivo RNAi-based scanning of the *Drosophila* genome to regulation of adipocyte cell fate in mammals.

INTRODUCTION

The world health organization (WHO) currently estimates that over 1 billion individuals worldwide are overweight. Almost one-third of these individuals are clinically obese, markedly raising their chances of cardiovascular disease, type 2 diabetes, cancer, and stroke (WHO, 2009). The regulation of body fat content in animals results from the integration of multiple nutrient, sensory, and hormonal inputs primarily at the level of the brain and adipose tissues (Farooqi and O'Rahilly, 2007). This integrative network is influenced not only by genetics but also by circadian rhythm and physical and social environments. Obesity is thus a complex, systems-level disease.

Spurned by the discovery of leptin (Zhang et al., 1994), tremendous progress has been made in identifying the molecular players and pathways regulating adiposity. The impressive bounds made through the study of gene-targeted mice (Speakman et al., 2008) and the tracking of monogenic obesity disorders in humans (Farooqi and O'Rahilly, 2007) have been complemented by studies in lower organisms (Gronke et al., 2005; Leopold and Perrimon, 2007; Schlegel and Stainier, 2007). Virtually all key metabolic regulators examined to date display conserved functions across phyla, including, for instance, insulin signaling, mTOR, and key lipases such as ATGL (Baker and Thummel, 2007; Gronke et al., 2005; Oldham and Hafen, 2003). Similar to mammals, model organisms such as

Drosophila melanogaster, Danio rerio, and *Caenorhabditis elegans* employ multiple molecular and tissue-based regulatory networks to balance energy needs, nutritional state, and aging and thus represent potent genomics tools for the study of metabolism. For instance, an RNAi feeding model was used to identify potential regulators of fat storage in the *C. elegans* genome (Ashrafi et al., 2003). More recent developments in functional genomics have now harnessed the potential of transgenic RNAi in *Drosophila* to allow both temporal and spatial control of RNAi knockdown at the whole-genome level (Dietzl et al., 2007).

RESULTS

An In Vivo High-Throughput Screen for Obesity Genes in *Drosophila*

To identify candidate obesity genes, we performed a genome-wide transgenic RNAi screen for fat content in adult *Drosophila* using a heat shock-inducible Hsp70-GAL4 system (Figure 1A). Triglycerides, the major lipid storage form in animals, were chosen as a direct measure of fly adiposity. Total fly triglyceride levels were measured by colorimetric determination and normalized to protein (Figure 1A). Using this experimental set-up, we were able to track triglyceride changes throughout development as well as to clearly distinguish sex-specific differences in fat content (Figure 1B; Figures S1A and S1B available online) and those induced by varying nutrient availability (Figure 1C). After the first round of screening, double-blinded analysis of RNAi lines targeting genes previously reported to regulate fat content revealed lipid alterations consistent with expected lean (Figure 1D) and obese (Figure 1E) phenotypes. Included were the LSD (*l*ipid *s*torage *d*roplet) and LPD (*lip*id *d*epleted) genes as well as the *Drosophila* insulin-like peptides (*Ilp*'s), the glucagon homolog *akh* and its receptor *akhr,* as well as *adipose (adp), bubblegum (bbg),* and the *Drosophila* SREBP homolog, *HLH106* (Gronke et al., 2007; Hader et al., 2003; Min and Benzer, 1999).

A Genome-wide Obesity Screen in Adult *Drosophila*

We tested the fat regulatory potential of 11,594 different UAS-RNAi transgenic lines corresponding to 10,812 transgene constructs and 10,489 distinct open reading frames (ORFs) in the adult fly (Table S1). Primary screening involved three rounds of testing where candidates with a Z score greater than 1.65 were selected for retesting (Figures 1A and 1F). After three rounds of selection 516 RNAi-transgenic lines remained, 462 of which had only single primary target predictions (S19 score $\geq$ 0.8 and $\leq$ 6 CAN repeats as described by Dietzl et al., 2007) (Table S2). Important for the translation of these findings into the mammalian context, 319 of 516 (62%) have human orthologs according to InParanoid, OrthoMCL, and Ensembl databases (Table S2).

Gene ontology (GO) based pathway analysis for *biological process* revealed enrichment of gene sets involved in cell fate determination, cellular protein metabolic processes, signal transduction, intracellular transport, and regulation of smoothened signaling (Figure 1G; Table S3). Pathways most depleted during the screen, i.e., those not relevant to fat regulation, included genes regulating behavior, cell cycle, organelle organization and biogenesis, locomotory behavior, and chromosome organization (Figure S1D). A network interaction assembly based on yeast-two-hybrid, text-mining, and pathway database information on the *Drosophila* hits and their mammalian orthologs revealed an interaction network map (Figure S2) highlighting genes of development, nutrient transport, cell-cycle regulation, the proteasome, protein translation, and chromatin remodeling. Of particular interest, the candidate gene list included a number of potential regulators of feeding control. For instance, six odorant and two gustatory receptor genes were targeted (odorant receptors10a, 56a, 65a, 67a, 83cd, and CG10407; gustatory receptors 98b and 36b). Also, the dopamine receptor *DopR2*, two octopamine receptors (*TyrR* and *oa2*), and the Nmda receptor-associated protein *Nmda1* all showed reduced body fat content following RNAi induction. In addition, altered fat deposition was observed in response to RNAi knockdown of known mediators of glucose/lipid mobilization including fructose-1,6-bisphosphatase (*fbp*), the two members of the glycerol phosphate shuttle (CG31169 and *Gpo-1*), mitochondrial acyl-carrier protein 1 (*mtacp1*), ADP/ATP translocase 2 (*Ant2*), pyruvate carboxykinase (CG1516), and fatty-acid synthetase (fasn). Also identified were the *Drosophila* orthologs of glucagon (*akh*), the insulin receptor (*dInR*), the downstream kinases PI3-kinase (*dPI3K*) and ribosomal-S6-kinase (*dRSK*), as well as the CREB-coactivator *dTORC*, and the critical TOR-signaling constituent *dTSC-1*. Of similar interest, *Drosophila* homologs of the critical early adipogenic regulators NCOR1/2, Jag1/2, and TAK1 (Ross et al., 2004; Suzawa et al., 2003; Yu et al., 2005) and the metabolic regulators CRTC1/2 and pyruvate carboxylase (PC) all showed marked alteration of the whole-body triglycerides (Altarejos et al., 2008; Koo et al., 2005; Zhang et al., 1995). We also hit the *Drosophila* lipoprotein *rfabg* (retinol fatty-acid binding glycoprotein) previously shown to transport key developmental morphogens such as *hedgehog* (Panakova et al., 2005). Indeed, "regulation of smoothened [hedgehog] signaling" was the most highly enriched signal transduction pathway in our GO analysis (Figure 1G; Table S3). Thus, our genome-wide approach identified multiple known molecular players previously associated with adipocyte development and function. Most importantly, the screen revealed a large number of candidate genes not previously associated with obesity.

Tissue-Specific Mapping of Candidate Obesity Genes

Considering the complexity of metabolism and the recognized diversity of tissue-specific processes that govern lipid storage (Leopold and Perrimon, 2007; Speakman et al., 2008), we set out to functionally categorize the candidate lipid regulators according to tissue specificity. RNAi lines of the 462 primary screen candidate genes were crossed to four independent GAL4 drivers with pan-neuronal (*nsyb*-GAL4*)*, muscle (*C57*-GAL4*)*, oenocyte (*oe*-GAL4*)*, and fat-body (*ppl*-GAL4) specificity, and their respective triglyceride levels determined (Figure 2A; Table S4). Interestingly, RNAi lines most strongly regulating fat content after pan-neuronal (*nsyb*-GAL4) knockdown elicited little or no change in fly triglyceride levels when induced in the muscle, oenocyte, or fat body (Figure 2B). Muscle-specific gene silencing (*C57*-GAL4), by contrast, enriched for genes that also elicited significant changes in triglycerides when targeted in oenocytes

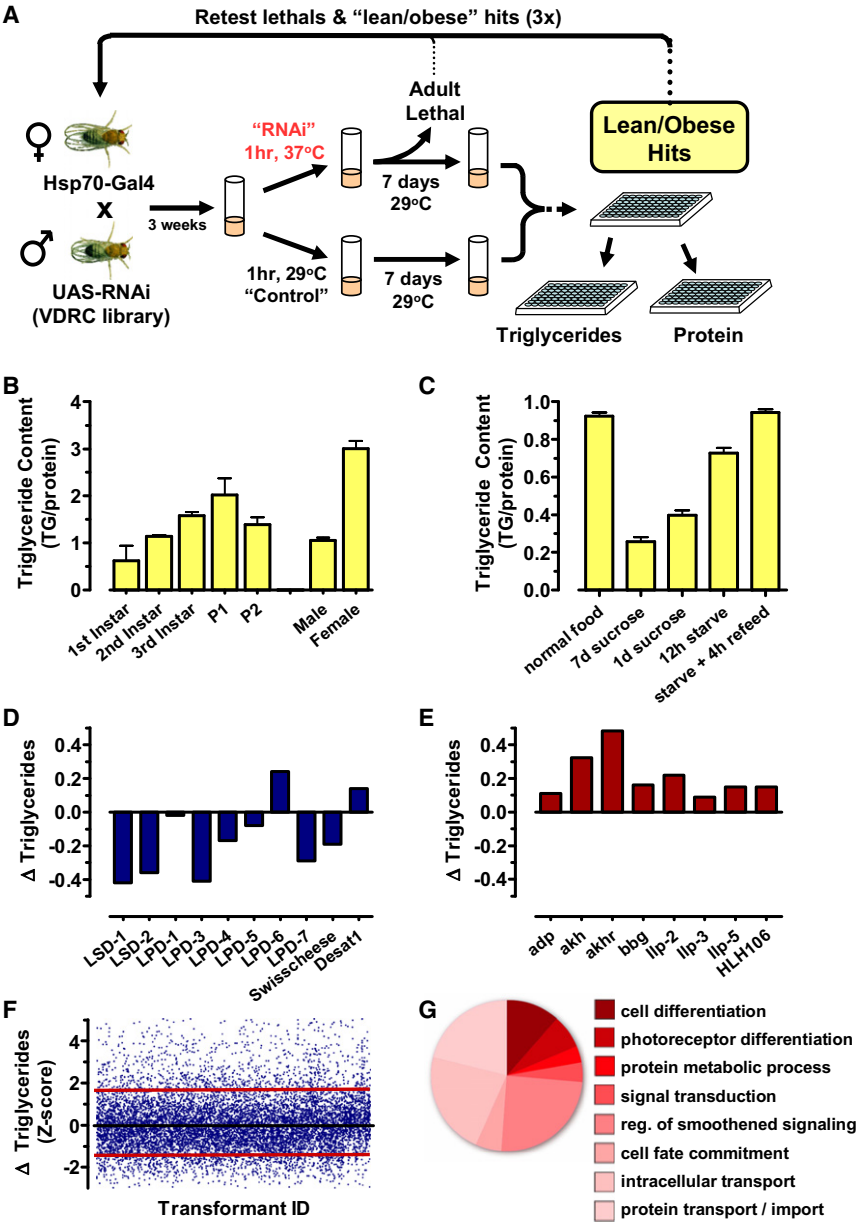

Figure 1. Genome-wide RNAi Screen for Obesity Factors in Adult *Drosophila* In Vivo

(A) Schematic of the screen design: virgin heat-shock-inducible (*Hsp70*-GAL4;*Tub*-GAL80^{ts}) females were crossed to UAS-RNAi transgenic males. RNAi was induced 2 days post-eclosure and again after 4 days. One week after RNAi induction, triglyceride and protein levels were determined in a 96-well format and compared to internal controls: noninduced progeny of the same cross.

(B) The system was capable of detecting developmental and sex-specific fat storage patterns and (C) a variety of feeding conditions. Data are shown as mean triglyceride content ± SEM, n = 8.

(D and E) Double-blinded retrieval of primary screen results for positive control lines predicted to (D) reduce or (E) increase triglyceride levels.

(F) Z score distribution of the primary screen results. Red lines indicate Z scores of +1.65 above and −1.65 below baseline levels.

(G) Gene ontology analysis with a level 5 cut-off for biological processes for all annotated genes with Z scores above or below ± 1.65 after three rounds of testing.

See also Figures S1 and S2.

and the fat body (Figure 2C). RNAi lines responding most substantially to oenocyte and fat-body-specific knockdown displayed a coordinate and reciprocal pattern of adiposity regulation (Figures 2D and 2E); these findings are in keeping with the tight regulatory interplay reported for these correlates of the mammalian adipose and liver (Gutierrez et al., 2007). GO analysis of the combined fat-enhancing and fat-diminishing gene sets for each of the four tissues tested are summarized in Figures 2B–2E and Tables S5, S6, S7, and S8. In support of the inducible design of the current screen, cell fate, cell differentiation, and organ development pathways showed strong enrichment in the analysis (Figures 2B–2E, right panels; Tables S5, S6, S7, and S8). Thus, we provide functional annotation of ~500 candidate obesity genes in four key metabolic tissues in *Drosophila*.

Neuronal Hits

In mammals, the leptin/AgRP/POMC axis exemplifies the profound neuronal dependency of feeding behavior, metabolic rate, insulin resistance, and, thus, obesity risk (Farooqi and O'Rahilly, 2007). Flies do not possess known homologs to this axis, but their feeding behavior is also neuronally anchored (Melcher et al., 2007). Approximately one-third of the primary screen hit list elicited triglyceride changes >25% when crossed with the neuronal *nsyb*-GAL4 driver (Table S5). A select number exhibited tight neuronal restriction in their response (Figure 3A). Included was the *Drosophila* homolog for SLC5A8 (CG8451; Figure 3A), a neuronal fatty-acid and lactate transporter (Martin et al., 2006). In rodents, fatty acids are sensed by neuronal processing of lactate generated by adjacent glial cells. Similarly, lines targeting homologs of glucagon (*akh,* neuronally secreted in *Drosophila*) and the neuronal Zn-transporter SLC39A10 both displayed tight neuronal responses. Also, TSC1 (*dTSC1*), a critical regulator of the amino acid-responsive TOR-signaling pathway, showed marked neuronal and fat-body-specific responsiveness (Figure 3D). It is an attractive hypothesis that aside from peripheral regulation of nutrient storage, TOR signaling in the central nervous system (CNS) might relay amino acid status to feeding behavior. Additional neuronal responsive targets likely to play a direct role in nutrient sensing included the odorant/gustatory receptors *Obp56a* and *TyR*. Thus, similar to mammals, fat storage in *Drosophila* appears regulated by a complex network of neuronal genes.

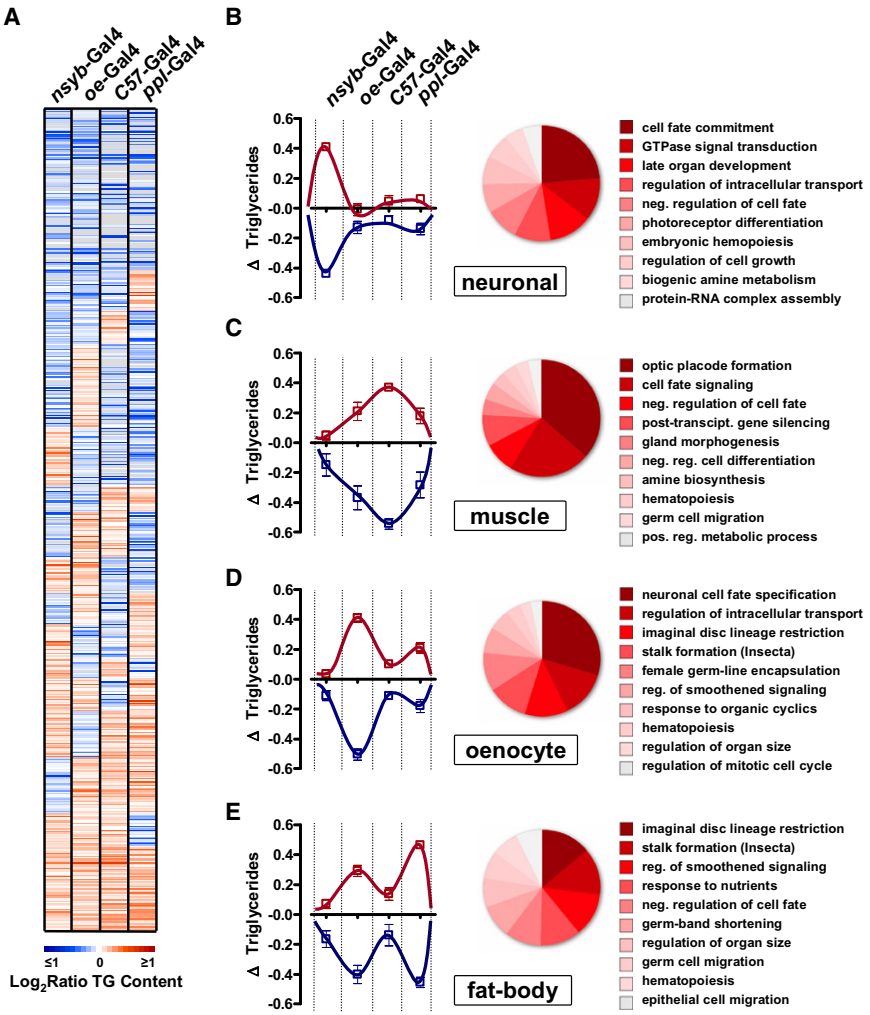

Figure 2. Tissue-Specific Regulation of Fat Storage

(A) Heat map of changes in triglyceride for primary screen hits crossed to *nsyb*-GAL4 (pan-neuronal), *oe*-GAL4 (oenocyte), *C57*-GAL4 (muscle), and *ppl*-GAL4 (fat-body) drivers. Changes are relative to control RNAi lines and isogenic w^{1118} flies crossed to the respective GAL4 drivers.

(B–E) Left panels show the mean changes in triglycerides after tissue-specific knockdown for the top-scoring fat-enhancing (red lines) and fat-depleting (blue lines) genes in each tissue category. Note the marked neuronal specificity, an overlap in fat-body and oenocyte responses, and a relative lack of specificity for top-scoring muscle-responsive genes. Right panels summarize gene-ontology analysis for each category (level 5 cut-off for biological processes). Intensity of the red reflects increased significance of the GO term.

Muscle Hits

Several genes showed tight muscle specificity (Figure 3B and Table S6), including homologs of the proline biosynthetic PYCR1 (*P5cr*), the glycogen debranching enzyme AGL (*CG9485*), and the *fbp* (fructose-1,6-bisphosphatase), a key regulator of glycolysis. Mevalonate decarboxylase (*CG8239*), which supports cholesterol biosynthesis and is currently being tested therapeutically to reduce cholesterol levels, showed similar muscle specificity as did the sterol-regulating enzyme ARV1 (*CG32442*). Mutants of ARV1 have previously been shown to exhibit altered lipid metabolism. Interestingly, genes involved in TLR signaling (*IM10*), the ribosome and protein translation (*CG3213*), proteolysis (*Fur1*), transcriptional regulation (*CG5591*), and microRNA-mediated silencing (*Smg5*) (Figure 3B) were also found to regulate triglyceride levels specifically in muscle cells.

Fat and Oenocyte Candidate Genes

The largest number of primary screen hits showed oenocyte- (*oe*-GAL4) and fat-body (*ppl*-GAL4) responses (Figures 3C and 3D; Tables S7 and S8). Interesting targets included homologs of inflammation-related genes: ARID2 (regulates interferon-responsive genes; Yan et al., 2005), *dTraf* (fly Traf-like protein), the pattern recognition receptor PGLYRP2, the interleukin enhancer-binding factor ILF2, the extracellular matrix protein tenascin (TNC), the ubiquitin-conjugating enzyme UBE2N (critical for TNF- and Toll-like-receptor signaling), or the deubiquitinating enzyme USP7. Additional components of the ubiquitin-ligase machinery were also revealed, namely UBR2, HERC4, and FBWX5 (also controls TSC1 and thus TOR signaling). Together these data support roles for immune regulatory networks and ubiquitination in fat storage regulation in *Drosophila*.

Oenocyte- and fat-body-specific knockdown analyses also identified genes involved in glycerol and lipid metabolism (Figures 3C and 3D; Tables S7 and S8). For instance, genes related to insulin signaling include the homologs of PP1 (inhibitory subunit 15b), S6KII, EIF2B, PI3K, and the insulin receptor (IR) itself. Also, direct mediators of lipid and glucose metabolism were identified, such as homologs of the ADP/ATP symporter ANT, NDUFAB1, GDPD, and GPD2. The latter, part of the glycerol-phosphate shuttle, regulates glycolytic rate and ROS production. Of interest, mice lacking GPD2 exhibit a 40% reduction in white adipose mass (Brown et al., 2002) and share a number of phenotypic features with deficiencies of glycerol kinase (GK), another enzyme found using the oenocyte-specific driver. In addition, we found *T3dh* (an iron-dependent regulator of fatty acid and ketone body metabolism), *Cyp6a2* (cytochrome P450 proteins catalyze numerous steps of cholesterol, steroids, and lipids synthesis), and the *Drosophila* homolog of the fatty-acid elongase ELOVL6 (which was particularly robust in both the oenocyte- and fat-body analyses). *Elovl6*$^{-/-}$ mice develop marked obesity and hepatosteatosis and show protection from hyperinsulinemia, hyperglycemia, and hyperleptinemia (Matsuzaka et al., 2007). Using fat-body-specific knockdown we also hit the *Drosophila* homolog of ELOVL7. Perhaps most importantly, we found multiple

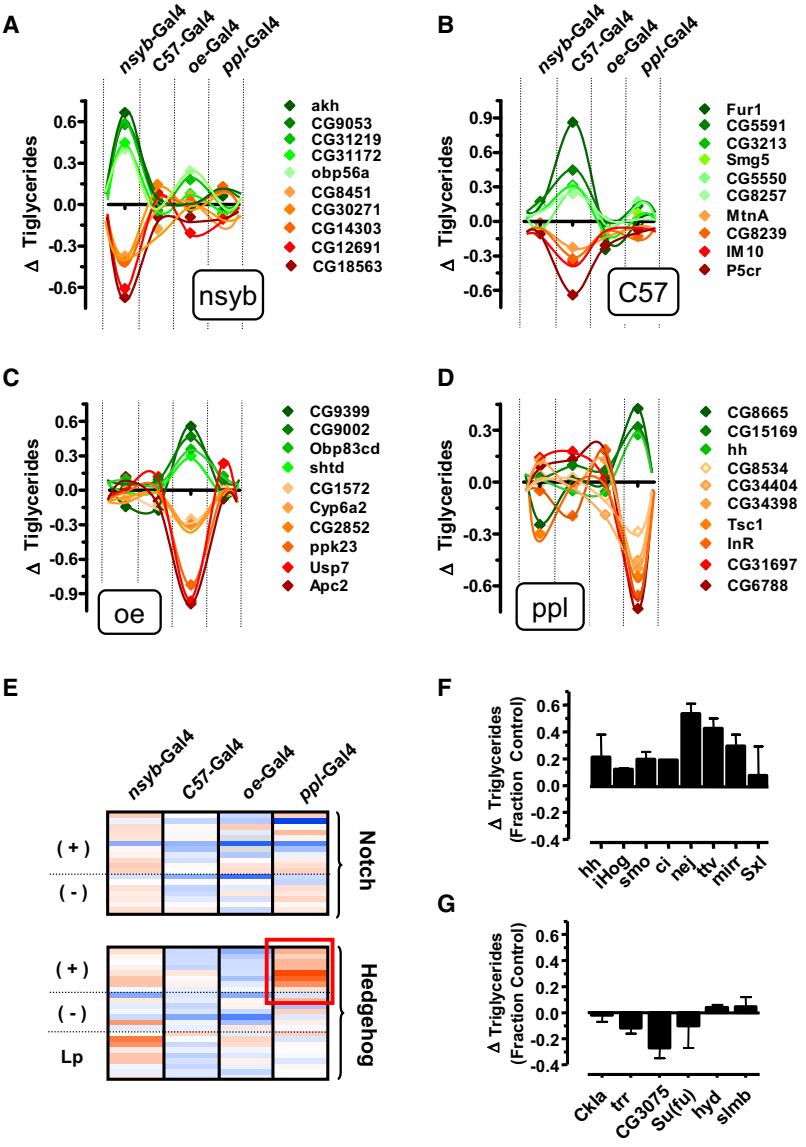

Figure 3. Analysis of Tissue Specificity Reveals Hedgehog Signaling as a Fat-Body-Specific Regulator of Triglyceride Levels

Triglyceride responses of candidate genes. Changes in adiposity in RNAi lines with the most tissue-restricted responses in the (A) pan-neuronal, (B) muscle, (C) oenocyte, and (D) fat-body compartments.

(E) Heat map of adiposity observed in UAS-RNAi transgenic fly lines targeting available annotated hedgehog and notch pathways. Changes are relative to averages of control RNAi lines and w^{1118} flies crossed to the respective GAL4 drivers. Genes are grouped according to their role as either positive (+) or negative (−) effectors, or as mediators of ligand processing and release (Lp). Red indicates increased triglycerides; blue indicates reduced triglycerides.

(F) Representative triglyceride changes in response to *ppl*-GAL4-driven knockdown of effectors of hedgehog signaling and (G) repressors of the pathway.

Data are presented as mean ± SEM, n = 4. *p < 0.05. See also Figure S3.

previously uncharacterized genes that regulate fat content in an oenocyte- and/or fat-body-dependent manner (Figures 3C and 3D). Thus, our screen has revealed a large number of general and tissue-specific candidate fly genes and multiple pathways that control triglyceride storage levels.

Hedgehog Is a Fat-Specific Obesity Pathway in *Drosophila*

The biological process "*regulation of smoothened [hedgehog] signaling*" was the top-scoring signal transduction pathway of all annotated pathways in the primary screen (Tables S3). An additional eight potential hedgehog signaling members recently identified in a *Drosophila* S2 cell screen for modulators of hedgehog signaling (Nybakken et al., 2005) were also hit in our primary obesity screen (Figure S2). Together these represent a >20-fold enrichment for the hedgehog signaling pathway. Importantly, hedgehog signaling scored third in fat-body-responsive pathways while not scoring at all in muscle or neuronal datasets (Figure 3E; Figure S3A).

Intriguingly, activators of the smoothened signaling pathway including the hedgehog ligand (*hh*), the binding protein *iHog*, the coreceptor *smoothened* (*smo*), the *nejire* coactivator (*nej*), the downstream transcription factors *cubits interuptus* (*ci*) and *mirror* (*mirr*), as well as *toutvelu* (*ttv*) and the hedgehog target *Sxl* all yielded increased triglycerides after *ppl*-GAL4 specified knockdown (Figure 3F). Conversely, decreased triglycerides levels were observed after knockdown of the known hedgehog repressors *trithorax-related* (*trr*), CG3075, and *Suppressor of Fused* (*Sufu*) (Figure 3G). Interestingly, whereas fat-body-specific knockdown of genes involved in processing or release of the hh ligand itself showed no coordinate effect on triglyceride levels (Figure 3E and Figure S3B), *nsyb*-GAL4-driven knockdown elicited mild elevation in triglycerides, suggesting that the hedgehog ligand may originate from a neuronal cell population (Figure 3E). As controls, knockdown of neither the effectors nor repressors of notch signaling showed any coordinate triglyceride response whereas knockdown of OXPHOS genes revealed coordinate fat-body and neuronal-specific reductions in triglyceride content (Figure 3E and Figures S3C and S3D), consistent with the fundamental role of the process in lipid flux. These data show that modulation of the hedgehog pathway in the fat body results in marked alterations in triglyceride levels.

cAMP, Glucocorticoid, and Hedgehog Crosstalk in White Adipogenesis

Our data show that the hedgehog pathway regulates triglyceride levels in adult *Drosophila*. A role for the hedgehog pathway has also been postulated in mammalian adipocyte biology both through systemic manipulation (Buhman et al., 2004) and in vitro (Suh et al., 2006). Cyclic AMP (cAMP) and dexamethasone

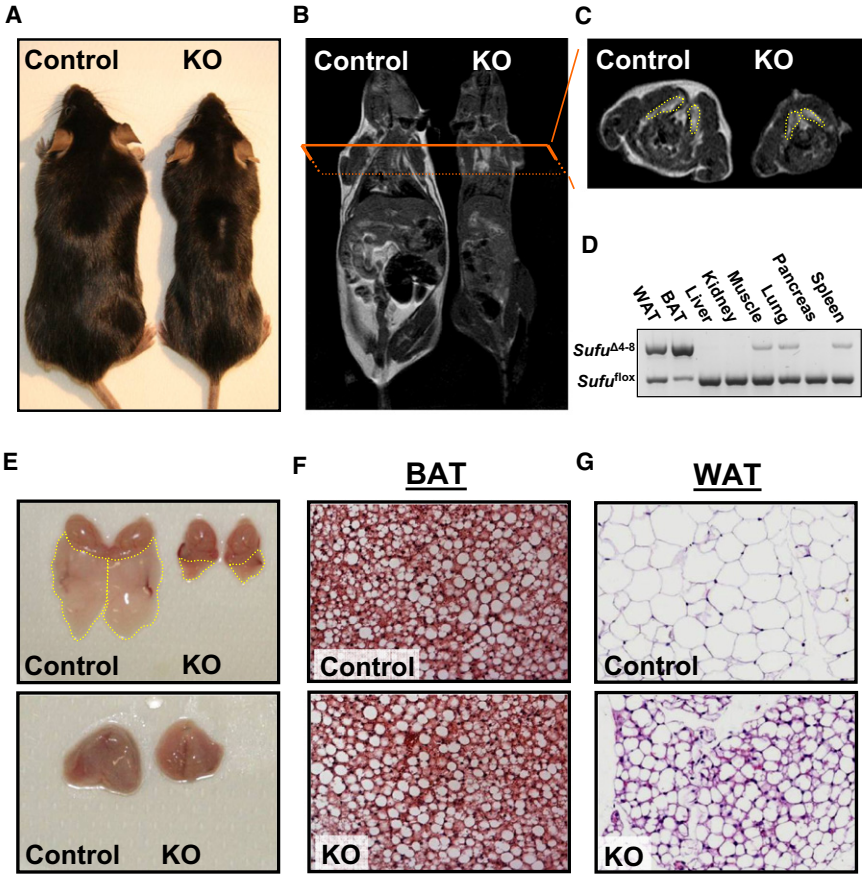

Figure 4. *aP2-Sufu* Mice Display White Adipose Tissue-Specific Lipoatrophy

(A) *aP2-Sufu*KO mice are born healthy and at Mendelian ratios.

(B) NMR imaging of an *aP2-Sufu*KO mouse and a Sufu-expressing littermate control.

(C) Cross-section at the level of the scapulae show unaltered brown adipose depots (yellow dashed lines).

(D) PCR revealed robust deletion of the Sufu allele ($Sufu^{\Delta 4\text{-}8}$) in both BAT and WAT depots. Minor deletion was detected in skeletal muscle, lung, and the spleen.

(E) Tissue dissection of white adipose tissue (WAT; upper panel) and brown adipose tissue (BAT; lower panel) revealed fully developed brown adipose depots despite severely compromised white adipose tissue depots in *aP2-Sufu*KO mice. Dashed lines mark white adipose tissue.

(F and G) Representative H&E stained sections of (F) brown (BAT) and (G) white (WAT) adipose tissues from *aP2-Sufu*KO and control littermate mice.

(H and I) Quantitative RT-PCR of the transcriptional hedgehog targets Gli1, Gli2, Ptch1, and Ptch2 confirmed activation of hedgehog signaling in both (H) WAT and (I) BAT of *aP2-Sufu*KO mice relative to targeted (flox) and aP2-cre (cre) transgenic littermate controls.

Data are presented as mean ± SEM. n = 5 mice per group. *$p < 0.05$. See also Figure S4.

(Dex), key inducers of differentiation in adipocyte cultures, have been shown to block hedgehog activation in several systems (Fan et al., 1995; Heine and Rowitch, 2009; Jiang and Struhl, 1995). Therefore, to establish a model system to investigate hedgehog signaling and adipogenesis, we subjected 3T3-L1 preadipocytes to two differentiation cocktails: a minimal induction medium containing insulin and troglitazone and the standard Dex and IBMX (increases cAMP) containing cocktail. We observed complete differentiation of 3T3-L1 cells under both culture conditions (Figure S4A). Importantly, in the presence of IBMX/Dex 3T3-L1, cells underwent complete differentiation whether in the presence or absence of the hedgehog activator Smoothened AGonist (SAG). Cells cultured in minimal induction medium, however, displayed a total block of differentiation upon addition of SAG (Figure S4A), suggesting that IBMX/Dex interferes with hedgehog stimulation. Expression of the hedgehog target genes Gli1 and Ptch1 showed that IBMX and Dex completely blocked induction of hedgehog activation, rendering SAG treatment ineffective (Figure S4B). Thus, hedgehog activation blocks white adipocyte differentiation solely in the absence of cAMP and glucocorticoid signaling.

Defective White but Normal Brown Adipose Tissue in Fat-Specific *Sufu* Mutant Mice

To assess the in vivo relevance of hedgehog signaling in mammalian adipogenesis, we generated fat-specific *Sufu* knockout animals (aP2-*Sufu*KO) (Figure S4C). Sufu is a potent endogenous inhibitor of hedgehog signaling in mammals (Jiang and Hui, 2008). $Sufu^{flox/flox}$ mice were crossed to the adipose tissue deleting aP2-Cre transgenic line (Figure S4C), and the resulting aP2-*Sufu*KO animals were born healthy and at Mendelian ratios. PCR amplification revealed target deletion in both white adipose tissue (WAT) and brown adipose tissue (BAT) (Figures 4A and 4D). aP2-*Sufu*KO mice displayed an immediate and obvious lean phenotype. MRI analysis revealed a significant and global reduction in white adipose tissue mass, including subcutaneous, perigonadal, and mesenteric depots (Figure 4B). Intriguingly, though, in contrast to the gross loss of WAT, cross-sectional examination of the interscapular region revealed fully developed BAT depots of both normal size and lipid content (Figures 4B and 4C). Direct measurement of WAT and BAT depot weights corroborated the divergent WAT/BAT phenotype, with an ~85%

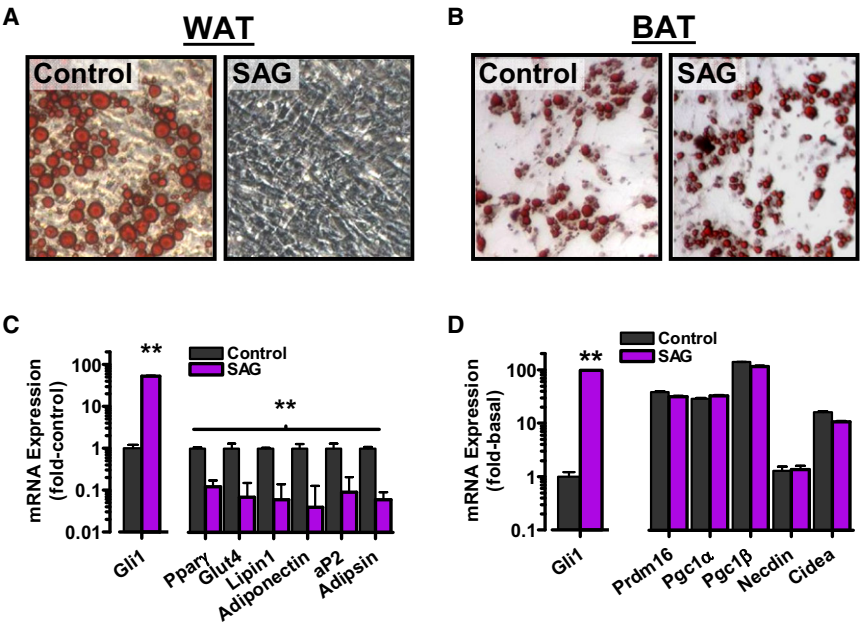

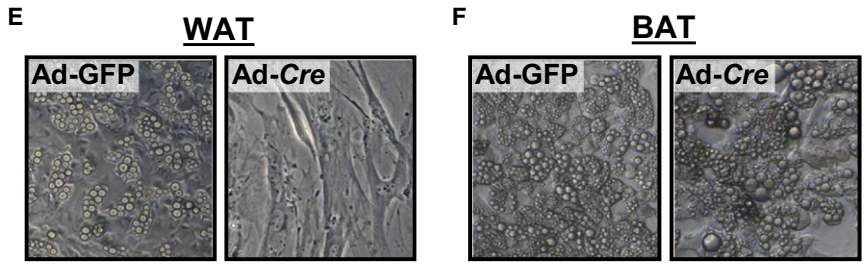

Figure 5. Hedgehog Signaling Specifically Blocks White Adipogenesis

(A and B) Microscopic view of Oil Red O-stained cell cultures reveals that activation of hedgehog signaling using SAG blocks differentiation of (A) white (WAT) but not (B) brown (BAT) primary murine adipocyte progenitors (stromal vascular cell, SVC, preparations). Data are from 12 days after induction using minimal induction medium (see Experimental Procedures).

(C) Quantitative RT-PCR 96 hr after induction of WAT-derived precursors reveals activation of hedgehog signaling (Gli1 expression) and reduction in WAT differentiation markers.

(D) BAT-derived precursors show no indication of altered differentiation after 96 hr of hedgehog activation. Data are mean ± SEM, n = 3–5 mice per group. $^{**}p < 0.01$.

(E) Phase-contrast images of primary WAT SVCs from $Sufu^{fl/fl}$ animals induced to differentiate using minimal induction medium after infection with Adeno-*Cre* or the Adeno-GFP control vector.

(F) Same as (E) but using primary brown adipose SVCs.

See also Figure S5.

reduction in perigonadal fat pad mass in *aP2-Sufu*KO mice concomitant with unaltered BAT mass (Figure 4E; Figure S4D). Tissue weight and histological analyses confirmed lack of any remarkable phenotype in multiple other tissues including pancreas and liver (no indication of steatosis), and muscle mass was unaffected (Figure S4D). Cutaneous adipose was also markedly diminished (Figure S4E). Whereas the morphology of *Sufu*-deficient BAT depots was largely indistinguishable from that of control animals (Figures 4E and 4F), examination of multiple WAT pads revealed marked and significant reductions in both adipocyte size (Figures 4E and 4G; Figure S4F) and total numbers (Figure S4G) in mutant animals. Of note, qPCR showed elevated Gli1, Gli2, and Ptch2 expression in both WAT (Figure 4H) and BAT (Figure 4I), verifying the intended pathway activation in both tissues. Thus, deletion of *Sufu* in fat tissue results in a markedly decreased white fat cell number and, remarkably, in normal brown adipose tissue.

Hedgehog Activation Blocks White but Not Brown Adipocyte Differentiation

Since the phenotype of *aP2-Sufu*KO mice suggested a defect in white adipocyte differentiation, we next stimulated 3T3-L1 "white" and HIB-1B "brown" adipocyte cell lines with SAG to induce hedgehog activation. Intriguingly, while robust block of 3T3-L1 differentiation was again observed (Figures S4A and S4B), HIB-1B cells showed no such response and underwent complete differentiation (not shown). These data were also confirmed using recombinant Sonic hedgehog (shh). Next, stromal vascular cell (SVC) fractions from both white and brown adipose depots were isolated from mice and stimulated with minimal induction cocktail in either the presence or absence of SAG. Activation of hedgehog signaling completely blocked adipogenesis in WAT-derived SVCs while showing no effect on BAT-derived SVCs (Figures 5A and 5B). qPCR analysis confirmed activation of hedgehog signaling in both the WAT- and BAT-derived SVC fractions and recapitulated on a transcriptional level the WAT-specific block in adipogenesis (Figures 5C and 5D and Figure S5A). To validate these findings, and to rule out differential kinetics of aP2-Cre expression between WAT and BAT in vivo, we isolated and tested SVC fractions from WAT and BAT of $Sufu^{flox/flox}$ activating the hedgehog pathway genetically, through administration of a Cre-recombinase containing adenovirus (Figures 5E and 5F; Figures S5B and S5C). Control (Adeno-GFP) and *Sufu*-deletion-induced (Adeno-Cre) SVCs derived from BAT showed equivalent and complete differentiation (Figure 5F; Figure S5C). Once again, WAT-derived SVCs differentiated only under control conditions, even after 12 days of induction (Figure 5E; Figure S5C). Thus, activation of hedgehog signaling in vivo and in vitro blocks white but not brown adipocyte differentiation.

Hedgehog Activation Dysregulates Early Adipogenic Factors

When we cross-referenced with literature focusing on adipogenesis, we found that an impressive 18 of 65 key regulators of

adipogenesis (Farmer, 2006; Gesta et al., 2007; Lefterova and Lazar, 2009; Rosen and MacDougald, 2006) had been described as Gli targets in other systems (Table S9). Intriguingly, when examined in 3T3-L1 preadipocytes, hedgehog activation induced a coordinated downregulation of the proadipogenic targets Bmp2, Bmp4, Egr2/Krox20, Sfrp1, and Sfrp2 by an average of ~50% after only 24 hr (Figure 6A). In contrast, quantification of the antiadipogenic target set showed upregulation of the multiple critical repressors (Nr2f2, Gilz, Hes1, and Ncor2); the negative regulators Jag1 and Pref1 remained unchanged at this time point (Figure 6B). Analysis of the master regulatory machinery downstream of these effectors revealed critical reductions in Pparγ, Cebpβ, and Cebpδ and increases in the antiadipogenic factors Cebpγ and Ddit3 (Figure 6C). Outside of this dramatic antiadipogenic profile, elevated levels of Cebpα were observed (Figure 6C). Importantly, a similar coordinate downregulation of Pparγ, Cebpβ, Cebpδ, as well as Cebpα was observed in WAT-derived SVCs following genetic activation of hedgehog signaling (Figure 6D).

To establish a direct link between hedgehog activation and adipogenic block in white adipose, in silico predictions were used to identify clusters of probable Gli-binding sites in the highly SAG-responsive genes Ncor2, Nr2f2, Sfrp2, and Hes1 (Figure S6A). To assess the functionality of these putative binding sites, we cloned the relevant promoter fragments and performed luciferase reporter assays (Figure 6E; Figure S6A; Tables S11 and S12). Gli1 and Gli2 induced activation of all Ncor2 and Nr2f2 reporter constructs, with the binding site clusters Ncor2_B, Nr2f2_A, and Nr2f2_B showing responses comparable to the hallmark target Ptch (Figure 6E). Further, chromatin immunoprecipitations on 3T3-L1 preadipocytes using Gli2- and Gli3-specifc antibodies revealed increases in Gli2 and Gli3 binding within the endogenous Ncor2, Hes1, Nr2f2, and Sfrp2 regulatory regions following SAG treatment. Together, these findings demonstrate endogenous Gli2/Gli3 binding to multiple adipogenic loci and implicate direct modulation of Ncor2 and Nr2f2 in the dysregulation of adipogenesis (Figure S6B).

Normal Glucose Tolerance and Insulin Sensitivity in *aP2-Sufu*KO Mice

To relate metabolic consequences of the unique WAT-specific lipoatrophy observed in our *aP2-Sufu*KO mice to previous models, we assessed glucose, insulin, and lipid tolerance, insulin sensitivity, and energy expenditure. Surprisingly, *aP2-Sufu*KO mice displayed normal glucose tolerance and glucose-induced insulin secretion during an oral glucose tolerance test (Figure 7A), and insulin tolerance testing was unremarkable (Figure S7A). In keeping with lack of apparent insulin resistance, *aP2-Sufu*KO showed no evidence of enhanced ectopic lipid accumulation. Further, euglycemic hyperinsulinemic clamps confirmed the lack of detectable insulin resistance, and interestingly, addition of tracers identified a tripling in glucose utilization within the residual white adipose tissue depot (Figures 7B and 7C). Measurement of key gluco-regulatory adipokines revealed a ~75% decrease in serum leptin levels and, unexpectedly, an increase in adiponectin levels (Figure 7D). Direct culture of freshly isolated BAT and WAT fragments from control and *aP2-Sufu*KO animals recapitulated this pattern with significantly

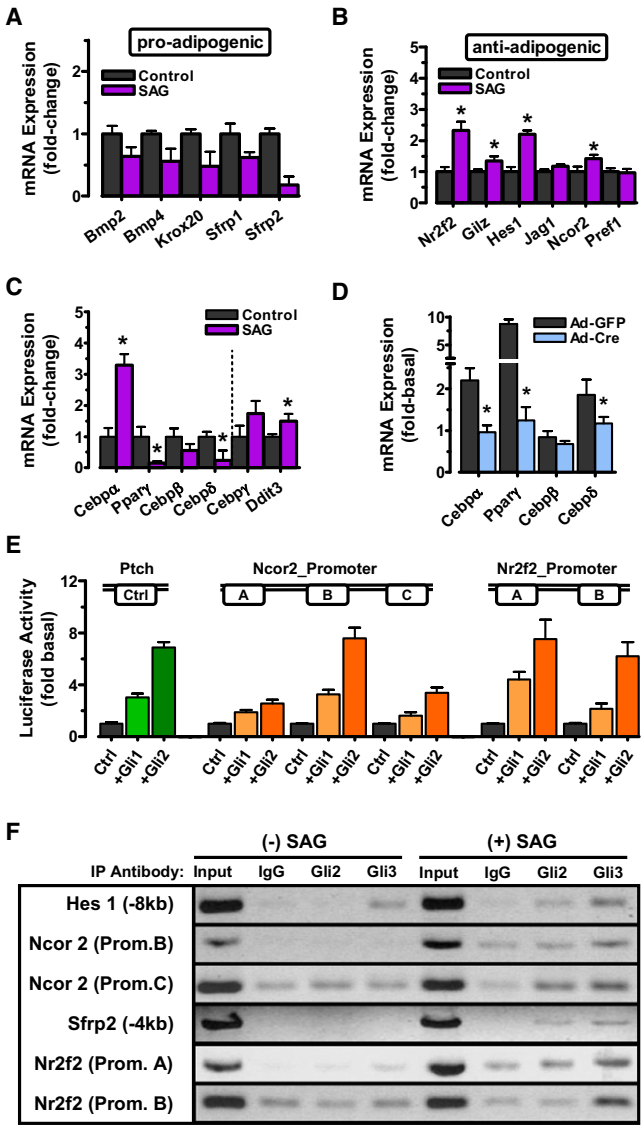

Figure 6. Hedgehog Signaling Blocks White Adipogenesis through Coordinate Repression of the Adipogenic Program

(A and B) Quantitative RT-PCR for known (A) proadipogenic and (B) antiadipogenic transcriptional hedgehog targets in 3T3-L1 cells 24–48 hr after induction in the absence (control) and presence of SAG (200 nM).

(C) Quantitative RT-PCR of the Pparγ-Cebpα adipogenic regulatory system in 3T3-L1 cells 96 hr after induction, in the presence or absence of SAG.

(D) Same as (C), but performed in primary WAT SVCs derived from *Sufu*$^{fl/fl}$ animals and induced to differentiate after infection with Adeno-*Cre* or an Adeno-GFP control vector.

(E) Luciferase reporter assays showing activation of Ncor2 and Nr2f2 promoter constructs in response to GLI1 or GLI2. The GLI target gene PTCH was used as positive control. Data are the mean of two experiments in triplicate.

(F) PCR analysis of chromatin immunoprecipitations of 3T3-L1 cells grown in the presence or absence of 200 nM SAG for 72 hr.

Data in (A)–(D) are presented as mean ± SEM, n = 3–5. *p < 0.05. See also Figure S6.

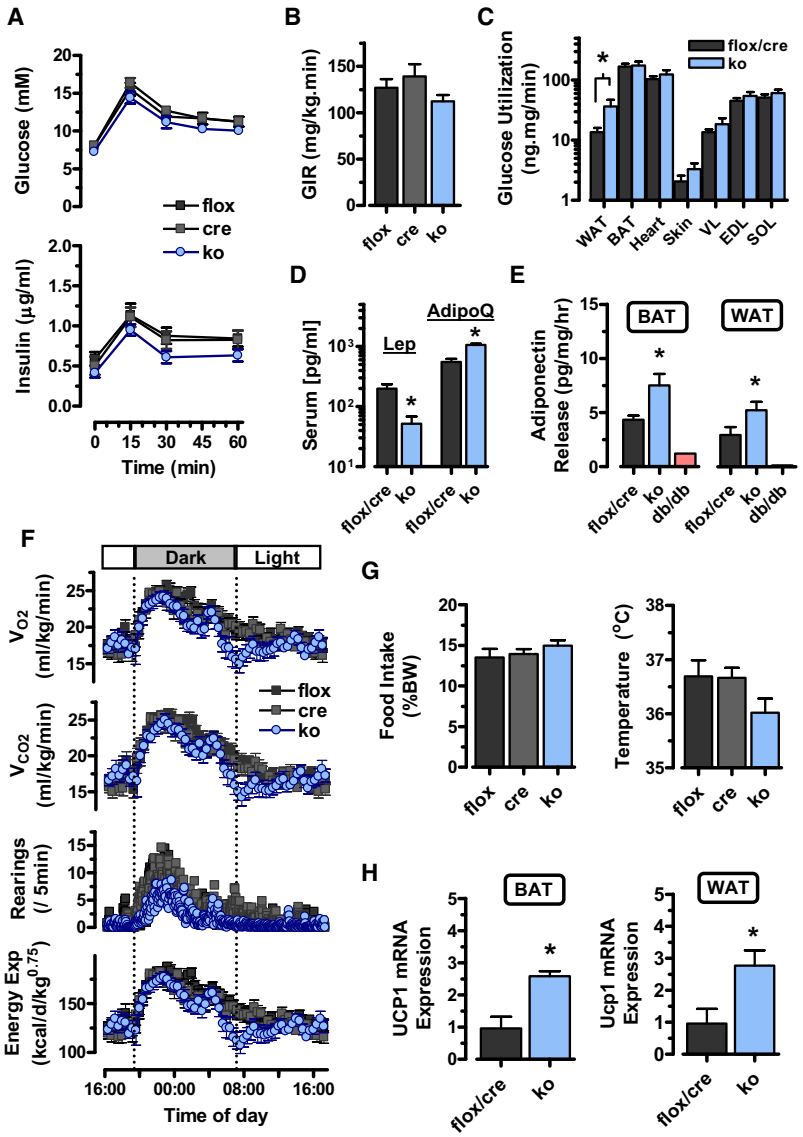

Figure 7. *aP2-Sufu*KO Mice Exhibit Normal Glucose and Energy Handling

(A) *aP2-Sufu*KO mice exhibit unaltered glucose handling during an oral glucose tolerance test (1 g/kg).

(B) Whole-body glucose infusion rate (GIR) was normal during euglycemic hyperinsulinemic clamp.

(C) Glucose tracing revealed enhanced glucose uptake in WAT of mutant mice but no differences in BAT, skin, cardiac, or skeletal muscles.

(D) Circulating serum leptin and adiponectin levels.

(E) In vitro culture of BAT and WAT fragments revealed increased adiponectin secretion in adipose of *aP2-Sufu*-KO mice.

(F) Indirect calorimetry in 10- to 12-week-old control and *aP2-Sufu*KO mice including O_2-consumption (VO_2), CO_2-production (VCO_2), and activity, as well as subsequent calculation of energy expenditure. Activity was measured as number of infrared beams broken with time.

(G) Food intake and body temperature measured at 12 weeks of age.

(H) Ucp1 expression in WAT determined by qPCR.

Data are mean ± SEM (n = 6–12). *p < 0.05. See also Figure S7.

reduced leptin (Figures S7C and S7D) and elevated adiponectin secretion (Figure 7E and Figure S7E). Thus, despite significant lipoatrophy, *aP2-Sufu*KO mice exhibit largely normal glucose homeostasis.

When tested using indirect calorimetry, little evidence was found of altered O_2-consumption or CO_2-production rates in the *aP2-Sufu*KO mice with exception of a short period of reduced gas exchange at the end of the dark cycle (Figure 7F; equivalent to a ~5% decrease in daily energy expenditure). Despite the marked differences in WAT and body weight (Figure S7F), *aP2-Sufu*KO mice showed no evidence of altered food intake relative to littermate controls (Figure 7G), respiratory quotient estimation suggested normal macronutrient partitioning (Figure S7G), and intestinal uptake and disposal of lipids were also normal (Figure S7H). What we did observe was markedly reduced activity in the *aP2-Sufu*KO animals during the dark cycle (Figure 7F). In the context of unaltered caloric intake and essentially normal energy expenditure, reduced activity suggests a significant shift in energy toward basal metabolic rate (BMR) or thermogenesis. O_2/CO_2 flux during periods of inactivity showed no evidence of increased BMR (Figure 7F). Direct measurement of body temperature showed a mild, albeit not significant, reduction in body temperature in the *aP2-Sufu*KO mice (Figure 7G, right panel), a somewhat paradoxical finding. Body temperature, however, only reflects thermogenesis in subjects of equivalent thermal state. *aP2-Sufu*KO mice exhibit little or no cutaneous (Figure S4E) and subcutaneous adipose stores (Figures 4B and 4C) and, therefore, at 22°C are under relative cold stress. Indeed, performing metabolic measurements at ambient temperature (22°C) can mask phenotypes as profound as obesity (Feldmann et al., 2009). Ucp1 mRNA levels measured in brown and white adipose tissue of our *aP2-Sufu*KO mice housed at 22°C were markedly elevated (Figure 7H), suggesting exaggerated thermal stress. We therefore analyzed body temperature, food intake, and body weight in littermate control and *aP2-Sufu*KO mice kept at 30°C (thermoneutrality) for a period of 1 month. Within 1 day at thermoneutrality, body temperature in *aP2-Sufu*KO mice normalized and even elevated slightly above controls (Figure S7I). Food intake also decreased in parallel with control littermates. Both food intake and body temperature shifts were maintained into a steady state (Figure S7I and not shown). Of note, oral glucose tolerance showed no deviation over this time period. Together these findings suggest that at ambient temperature *aP2-Sufu*KO mice divert bulk energy toward thermogenesis explaining at least in part the observed reduction in activity. Thus, *aP2-Sufu*KO mice exhibit WAT-specific lipoatrophy, normal glucose tolerance, and largely normal regulation of energy expenditure.

DISCUSSION

The power of *D. melanogaster* RNAi transgenics to probe gene function on a genome-wide scale has allowed us to screen ~78% coverage of the *Drosophila* genome. One significant advantage of our inducible approach employed here is the ability to interrogate the fat regulatory potential of the ~30% of the *Drosophila* genome that is developmentally lethal under classic mutation conditions. Indeed, the result that cell differentiation genes scored as the most enriched ontology subcategory substantiates the inducible strategy employed and identifies a large number of developmentally lethal genes with strong lipid storage regulatory potential. Consistent with a previous feeding-induced RNAi *C. elegans* screen, the fraction of candidate genes resulting in decreased fat content upon knockdown (360 of 516; 70%) exceeded that of obesity-causing candidates (216 of 516; 30%), which is consistent with the hypothesis that the major evolutionary pressures for animals have been to favor nutrient storage. Our screen identified a large number of genes already known to play a key role in mammalian fat or lipid metabolism, including enzymes of membrane lipid biosynthesis, fatty acid and glucose metabolism, and sterol metabolism. Further, our whole-genome screen has uncovered a plethora of additional candidate genes of adiposity regulation, a large proportion of which had no previous annotated biological function. Moreover, we identified multiple genes that either positively or negatively regulate whole fly triglyceride levels when targeted specifically in neurons, the fly liver (oenocyte), the fat body, or muscle cells. Analyses of the hits allowed us to define either gene sets that function globally in all these tissues or others that display coordinate regulation of adiposity when targeted in metabolically linked organs such as the fat and the liver. Since >60% of the candidate genes are conserved across phyla to humans, our data set is a unique starting point for the elucidation of novel regulatory modalities in mammals.

The top-scoring signal transduction pathway in our GO-based enrichment analysis was the hedgehog pathway. Tissue-specificity assessment revealed further that this enrichment was primarily derived from a pronounced fat-body restriction in function. Hedgehog signaling has been previously implicated in adipose tissue biology (Suh et al., 2006; Wu et al., 2002; Zehentner et al., 2000). In *Drosophila* larvae, hedgehog activation reduces lipid content consistent with what we found in adult flies and our fat-specific fly knockdown lines (Suh et al., 2006). Similarly, knockdown of the *C. elegans* equivalent of the inhibitory hedgehog receptor Ptch results in a prominent adiposity reducing phenotype in a feeding-based RNAi screen (Ashrafi et al., 2003). We therefore homed into the hedgehog pathway to provide proof of principle for the fly screen and to translate our *Drosophila* results directly into the mammalian context.

Several reports exist describing systemic manipulation of hedgehog signaling, either by injection of ligand-depleting antibody or through examination of a systemic hypomorphic mutant, the $Ptch^{mes/mes}$ mouse (Buhman et al., 2004; Makino et al., 2001). Indeed $Ptch^{mes/mes}$ mice display largely normal white adipose tissue depots albeit reduced in size (Li et al., 2008). Hedgehog signaling plays a crucial role in multiple organs systems including at least one intimately involved in nutrient storage and the etiologies of obesity and insulin resistance, namely, the pancreatic islet (Hebrok et al., 2000; Thomas et al., 2000). Our in vitro and in vivo data using the adipose-specific *Sufu* mutant mice clearly show that hedgehog activation results in a complete and cell-autonomous inhibition of white adipocyte differentiation. The residual white adipose tissue observed in our *aP2-Sufu*KO mice is most likely due to late inefficient deletion and/or is due to developmental timing effects. Indeed, aP2 (and thus aP2-Cre) are expressed relatively late during adipocyte differentiation (Gesta et al., 2007). The remarkable finding was that genetic activation of hedgehog signaling in vivo and in vitro blocks only white but not brown adipocyte differentiation.

Fat is mainly stored in two cell types: WAT, which is the major storage site for triglycerides, and BAT, which, through the burning of lipids to heat (through uncoupling of mitochondrial oxidative phosphorylation), serves to regulate body temperature (Farmer, 2009). Recent PET-CT data have revealed that adult humans contain functional BAT and that the amount of BAT is inversely correlated with body mass index (Cypess et al., 2009; van Marken Lichtenbelt et al., 2009; Virtanen et al., 2009; Zingaretti et al., 2009). These new data in humans rekindle the notion that a functional BAT depot in humans could represent a potent therapeutic target in the context of obesity control. Lineage tracking and genetic studies have shown that WAT and interscapular BAT cells derive from two different but related progenitor pools (Seale et al., 2009; Tseng et al., 2008). Our genetic data now demonstrate both in vitro and in vivo that hedgehog activation results in a virtually complete block of WAT development but leaves the differentiation process of brown adipocytes wholly intact. These data further support the concept that white and brown adipocytes are derived from distinct precursor cells.

To the best of our knowledge *aP2-Sufu*KO mice are the first white adipose-specific lipoatrophic mice with a fully functional BAT depot over the long-term and normal glucose tolerance and insulin sensitivity. The capacity of an intact BAT depot to burn energy in *aP2-Sufu*KO mice likely underlies, at least in part, their lack of ectopic lipid accumulation and insulin resistance. This largely normal metabolic picture highlights the potent regulatory capacity of brown adipose tissue and should prove invaluable in understanding the distinct roles of brown and white adipose tissues.

EXPERIMENTAL PROCEDURES

Fly Screening

For detailed experimental procedures, please see the Extended Experimental Procedures. Male UAS-RNAi transgenic flies were obtained from the Vienna *Drosophila* RNAi Centre (VDRC) and crossed with *Hsp70*-GAL4;*Tub*-$GAL80^{ts}$ virgins and the progeny transferred to new vials after 3 weeks. Flies were heat-shocked immediately and after 4 days. On day 7, flies were manually crushed, sonicated, heat-inactivated, and centrifuged and the supernatant used for 96-well based colorimetric determination of triglycerides (GPO Trinder, Sigma) and protein (BCA, Pierce). Tissue-specific secondary screen followed a parallel procedure without heat-shock and controlled against w^{1118} wild-types and a random set of RNAi lines shown to exhibit no phenotype.

Data Analysis and Ortholog Retrieval

Orthologs were retrieved from InParanoid, OrthoMCL, and Ensembl. Gene Ontology analysis used GoStat with a Benjamini and Hochberg correction

using the online GOToolbox application. Network maps were generated using cytoscape and based on online protein interaction databases.

Generation of *Sufu* Mutant Mice

Conditional *Sufu* mice were generated by the laboratory of C.-c.H. (unpublished data). Adipose-specific *Sufu* knockout mice were generated by crossing conditional $Sufu^{fl/fl}$ mice with *aP2*-Cre transgenic mice (R. Evans; JAX). Cre recombinase-positive wild-type and Cre recombinase-negative $Sufu^{fl/fl}$ littermates served as controls.

Euglycemic Hyperinsulinemic Clamp, Tissue Glucose Utilization, and Indirect Calorimetry

Indirect calorimetry was performed for 72 hr using an open-circuit, indirect calorimetry system including spontaneous activity by beam breaking (Oxylet, Panlab-Bioseb). Euglycemic hyperinsulinemic clamp studies were performed on conscious mice 5 days insertion of a femoral catheter and after a 6 hr fast. D-[3-^{3}H]-glucose and ^{3}H-2-deoxyglucose (tissue-specific utilization) were used as tracers and insulin was infused at 18 mU/kg/min. Euglycemia was maintained by variable infusion of 15% glucose. Calculations were based on blood sampled at steady state (T = 120–180 min). Total radioactivity was determined by scintillation counting, and glucose concentrations by the glucose oxidase method (BioMerieux).

Histology, Adipocyte Size, and Number

For staining of neutral lipids, cells were fixed and stained with Oil Red O (OrO) according to standard procedures. Adipocyte number and size analyses were performed using H&E-stained paraffin sections of perigonadal WAT pads by semi-automated morphometry. Definiens software suite was used for the automated determination of adipocyte size and number from multiple intervalled histological sections.

Isolation of Mouse Primary Brown and White Preadipocytes

Primary preadipocytes were obtained by collagenase digestion from perigonadal white and interscapular brown adipose tissue depots in mice. Isolated cells were plated in DMEM/F12 containing 10% FBS. On the next day, and to remove most of the contaminating macrophages, adherent cells were trypsinized and transferred to experimental dishes at a density of 15,000 cells/cm^2. Sca-1$^+$CD31$^-$Lin$^-$ primary white and brown preadipocytes were facs sorted from adipose stromal cell preparations immediately after collagenase digestion.

Cell Culture and Adipocyte Differentiation

Murine 3T3-L1 preadipocytes (ATCC) and HIB-1B cells, kindly provided by Bruce Spiegelman, were propagated in DMEM containing 10% calf and fetal bovine serum, respectively. Mouse primary cells were expanded in DMEM/F12 supplemented with 10% FBS. For adipocyte differentiation experiments, cells were differentiated and maintained in an IBMX/dexamethasone-free minimal induction medium including insulin, T3, biotin, pantothenic acid, and troglitazone, with the exception of those exploring the effects of IBMX and Dex (Figure S4). Recombinant sonic hedgehog (Shh; 300 ng/ml; R&D Systems) or SAG (200 nM; Alexis) were added to the cells as indicated. All chemicals for cell culture were obtained from Sigma unless otherwise indicated.

Excision of $Sufu^{fl/fl}$ in Primary Adipocyte Progenitors

For adenoviral infection of primary white and brown fat precursors, near confluent cultures of SVC fractions of perigonadal white and interscapular brown adipose tissue depots were infected overnight with either Ad5-eGFP or Ad5-Cre-IRES-GFP. One day after infection, the medium was replaced and cells were maintained in complete growth medium for an additional 24 hr before inducing differentiation.

Quantitative RT-PCR

For quantitative PCR (qRT-PCR), analysis of total RNA was performed on an AbiPRISM 7900HT real-time cycler (Applied Biosystems) using iQ SYBR Green Supermix (Bio-Rad). Threshold cycles (C_t-values) of all replicate analyses were normalized to acidic ribosomal phosphoprotein P0 (Rplp0/36B4). To compare the effect of various treatments with untreated controls, $2^{-\Delta\Delta Ct}$ values were calculated to obtain fold expression levels. Primers are listed in Table S8.

Western Blot

Proteins were extracted by homogenizing in RIPA buffer containing protease inhibitors (Complete Mini, Roche). Adipose tissue homogenates were resolved by SDS-PAGE, transferred to PVDF membranes (GE Healthcare), and probed with anti-Sufu and anti-Hsc70 antibodies (Santa Cruz Biotechnology).

In Silico Gli Target Analysis, Luciferase Assays, and ChIP Analysis

Genomic sequences including 10 kb upstream of mouse Ncor2, Nr2f2, Hes1, and Sfrp2 were analyzed for putative Gli-binding sites using ScanAce. Luciferase reporter plasmids were assembled from Gli-binding site clusters of Ncor2 and Nr2f2 cloned into pGL3-basic vector (Promega). Restriction sites and primer sequences are given in Table S12. 3T3-L1 cells were cotransfected with Gli effector plasmids or empty vector control and luciferase activity measured 48 hr post-transfection. For chromatin immunoprecipitation, chromatin was isolated from 3T3-L1 cells treated for 72 hr with or without SAG (200 nM) using the SimpleChIP Enzymatic ChIP kit (Cell Signaling Technology). ChIP assays were performed using the ChIP-IT (Active Motif) and IgG (Active Motif) used as a negative control. Anti-Gli2 (Abcam) and anti-Gli3 (Santa Cruz) rabbit polyclonal antibodies were used to immunoprecipitate the DNA/protein complex. Crosslink reversed samples were treated with Proteinase K and the DNA purified and analyzed using PCR. A primer list and promoter maps are included in Table S13 and Figure S6.

Statistical Analyses

All data unless otherwise indicated are shown as mean values ± standard error of the mean (SEM) and tested statistically using two-tailed Student's t test or ANOVA. All figures and statistical analyses were generated using GraphPad Prism 4. $p < 0.05$ was considered to indicate statistical significance.

SUPPLEMENTAL INFORMATION

Supplemental Information includes Extended Experimental Procedures, seven figures, and thirteen tables and can be found with this article online at doi:10.1016/j.cell.2009.12.027.

ACKNOWLEDGMENTS

The authors are indebted to the IMBA and MUW service departments, all members of the VDRC Drosophila library, and Barry Dickson, Pawel Pasierbek, Maria Novatchkova, Patricia Schittenhelm, Helen Damhofer, and Maria Ozsvar-Kozma for excellent technical help. J.A.P. was supported by fellowships from the JDRF and the Marie-Curie Foundation. This project, J.A.P., and H.E. are supported by the WWTF. C.-C.H. was supported by CIHR and CCSRI. J.M.P. is supported by the Austrian Academy of Sciences, GEN-AU (Genome Austria), the Austrian Ministry of Science and Education, and a European Union Advanced ERC grant. P.D.C. is a research associate from the FRS-FNRS Belgium. D.F. is supported by the CNRS and a Droselegans grant from the Programme MIME, and the D.F. laboratory is an "Equipe FRM" (Fondation pour la Recherche Médicale).

Received: May 22, 2009
Revised: September 30, 2009
Accepted: December 4, 2009
Published: January 7, 2010

REFERENCES

Altarejos, J.Y., Goebel, N., Conkright, M.D., Inoue, H., Xie, J., Arias, C.M., Sawchenko, P.E., and Montminy, M. (2008). The Creb1 coactivator Crtc1 is required for energy balance and fertility. Nat. Med. *14*, 1112–1117.

Ashrafi, K., Chang, F.Y., Watts, J.L., Fraser, A.G., Kamath, R.S., Ahringer, J., and Ruvkun, G. (2003). Genome-wide RNAi analysis of Caenorhabditis elegans fat regulatory genes. Nature *421*, 268–272.

Baker, K.D., and Thummel, C.S. (2007). Diabetic larvae and obese flies-emerging studies of metabolism in Drosophila. Cell Metab. *6*, 257–266.

Brown, L.J., Koza, R.A., Marshall, L., Kozak, L.P., and MacDonald, M.J. (2002). Lethal hypoglycemic ketosis and glyceroluria in mice lacking both the mitochondrial and the cytosolic glycerol phosphate dehydrogenases. J. Biol. Chem. *277*, 32899–32904.

Buhman, K.K., Wang, L.C., Tang, Y., Swietlicki, E.A., Kennedy, S., Xie, Y., Liu, Z.Y., Burkly, L.C., Levin, M.S., Rubin, D.C., et al. (2004). Inhibition of Hedgehog signaling protects adult mice from diet-induced weight gain. J. Nutr. *134*, 2979–2984.

Cypess, A.M., Lehman, S., Williams, G., Tal, I., Rodman, D., Goldfine, A.B., Kuo, F.C., Palmer, E.L., Tseng, Y.H., Doria, A., et al. (2009). Identification and importance of brown adipose tissue in adult humans. N. Engl. J. Med. *360*, 1509–1517.

Dietzl, G., Chen, D., Schnorrer, F., Su, K.C., Barinova, Y., Fellner, M., Gasser, B., Kinsey, K., Oppel, S., Scheiblauer, S., et al. (2007). A genome-wide transgenic RNAi library for conditional gene inactivation in Drosophila. Nature *448*, 151–156.

Fan, C.M., Porter, J.A., Chiang, C., Chang, D.T., Beachy, P.A., and Tessier-Lavigne, M. (1995). Long-range sclerotome induction by sonic hedgehog: direct role of the amino-terminal cleavage product and modulation by the cyclic AMP signaling pathway. Cell *81*, 457–465.

Farmer, S.R. (2006). Transcriptional control of adipocyte formation. Cell Metab. *4*, 263–273.

Farmer, S.R. (2009). Obesity: Be cool, lose weight. Nature *458*, 839–840.

Farooqi, I.S., and O'Rahilly, S. (2007). Genetic factors in human obesity. Obes. Rev. *8* (*Suppl 1*), 37–40.

Feldmann, H.M., Golozoubova, V., Cannon, B., and Nedergaard, J. (2009). UCP1 ablation induces obesity and abolishes diet-induced thermogenesis in mice exempt from thermal stress by living at thermoneutrality. Cell Metab. *9*, 203–209.

Gesta, S., Tseng, Y.H., and Kahn, C.R. (2007). Developmental origin of fat: tracking obesity to its source. Cell *131*, 242–256.

Gronke, S., Mildner, A., Fellert, S., Tennagels, N., Petry, S., Muller, G., Jackle, H., and Kuhnlein, R.P. (2005). Brummer lipase is an evolutionary conserved fat storage regulator in *Drosophila*. Cell Metab. *1*, 323–330.

Gronke, S., Muller, G., Hirsch, J., Fellert, S., Andreou, A., Haase, T., Jackle, H., and Kuhnlein, R.P. (2007). Dual lipolytic control of body fat storage and mobilization in Drosophila. PLoS Biol. *5*, e137.

Gutierrez, E., Wiggins, D., Fielding, B., and Gould, A.P. (2007). Specialized hepatocyte-like cells regulate Drosophila lipid metabolism. Nature *445*, 275–280.

Hader, T., Muller, S., Aguilera, M., Eulenberg, K.G., Steuernagel, A., Ciossek, T., Kuhnlein, R.P., Lemaire, L., Fritsch, R., Dohrmann, C., et al. (2003). Control of triglyceride storage by a WD40/TPR-domain protein. EMBO Rep. *4*, 511–516.

Hebrok, M., Kim, S.K., St Jacques, B., McMahon, A.P., and Melton, D.A. (2000). Regulation of pancreas development by hedgehog signaling. Development *127*, 4905–4913.

Heine, V.M., and Rowitch, D.H. (2009). Hedgehog signaling has a protective effect in glucocorticoid-induced mouse neonatal brain injury through an 11betaHSD2-dependent mechanism. J. Clin. Invest. *119*, 267–277.

Jiang, J., and Hui, C.C. (2008). Hedgehog signaling in development and cancer. Dev. Cell *15*, 801–812.

Jiang, J., and Struhl, G. (1995). Protein kinase A and hedgehog signaling in *Drosophila* limb development. Cell *80*, 563–572.

Koo, S.H., Flechner, L., Qi, L., Zhang, X., Screaton, R.A., Jeffries, S., Hedrick, S., Xu, W., Boussouar, F., Brindle, P., et al. (2005). The CREB coactivator TORC2 is a key regulator of fasting glucose metabolism. Nature *437*, 1109–1111.

Lefterova, M.I., and Lazar, M.A. (2009). New developments in adipogenesis. Trends Endocrinol. Metab. *20*, 107–114.

Leopold, P., and Perrimon, N. (2007). Drosophila and the genetics of the internal milieu. Nature *450*, 186–188.

Li, Z., Zhang, H., Denhard, L.A., Liu, L.H., Zhou, H., and Lan, Z.J. (2008). Reduced white fat mass in adult mice bearing a truncated Patched 1. Int. J. Biol. Sci. *4*, 29–36.

Makino, S., Masuya, H., Ishijima, J., Yada, Y., and Shiroishi, T. (2001). A spontaneous mouse mutation, mesenchymal dysplasia (mes), is caused by a deletion of the most C-terminal cytoplasmic domain of patched (ptc). Dev. Biol. *239*, 95–106.

Martin, P.M., Gopal, E., Ananth, S., Zhuang, L., Itagaki, S., Prasad, B.M., Smith, S.B., Prasad, P.D., and Ganapathy, V. (2006). Identity of SMCT1 (SLC5A8) as a neuron-specific Na+-coupled transporter for active uptake of L-lactate and ketone bodies in the brain. J. Neurochem. *98*, 279–288.

Matsuzaka, T., Shimano, H., Yahagi, N., Kato, T., Atsumi, A., Yamamoto, T., Inoue, N., Ishikawa, M., Okada, S., Ishigaki, N., et al. (2007). Crucial role of a long-chain fatty acid elongase, Elovl6, in obesity-induced insulin resistance. Nat. Med. *13*, 1193–1202.

Melcher, C., Bader, R., and Pankratz, M.J. (2007). Amino acids, taste circuits, and feeding behavior in Drosophila: towards understanding the psychology of feeding in flies and man. J. Endocrinol. *192*, 467–472.

Min, K.T., and Benzer, S. (1999). Preventing neurodegeneration in the Drosophila mutant bubblegum. Science *284*, 1985–1988.

Nybakken, K., Vokes, S.A., Lin, T.Y., McMahon, A.P., and Perrimon, N. (2005). A genome-wide RNA interference screen in Drosophila melanogaster cells for new components of the Hh signaling pathway. Nat. Genet. *37*, 1323–1332.

Oldham, S., and Hafen, E. (2003). Insulin/IGF and target of rapamycin signaling: a TOR de force in growth control. Trends Cell Biol. *13*, 79–85.

Panakova, D., Sprong, H., Marois, E., Thiele, C., and Eaton, S. (2005). Lipoprotein particles are required for Hedgehog and Wingless signalling. Nature *435*, 58–65.

Rosen, E.D., and MacDougald, O.A. (2006). Adipocyte differentiation from the inside out. Nat. Rev. *7*, 885–896.

Ross, D.A., Rao, P.K., and Kadesch, T. (2004). Dual roles for the Notch target gene Hes-1 in the differentiation of 3T3-L1 preadipocytes. Mol. Cell. Biol. *24*, 3505–3513.

Schlegel, A., and Stainier, D.Y. (2007). Lessons from "lower" organisms: what worms, flies, and zebrafish can teach us about human energy metabolism. PLoS Genet. *3*, e199.

Seale, P., Kajimura, S., and Spiegelman, B.M. (2009). Transcriptional control of brown adipocyte development and physiological function–of mice and men. Genes Dev. *23*, 788–797.

Speakman, J., Hambly, C., Mitchell, S., and Krol, E. (2008). The contribution of animal models to the study of obesity. Lab. Anim. *42*, 413–432.

Suh, J.M., Gao, X., McKay, J., McKay, R., Salo, Z., and Graff, J.M. (2006). Hedgehog signaling plays a conserved role in inhibiting fat formation. Cell Metab. *3*, 25–34.

Suzawa, M., Takada, I., Yanagisawa, J., Ohtake, F., Ogawa, S., Yamauchi, T., Kadowaki, T., Takeuchi, Y., Shibuya, H., Gotoh, Y., et al. (2003). Cytokines suppress adipogenesis and PPAR-gamma function through the TAK1/TAB1/NIK cascade. Nat. Cell Biol. *5*, 224–230.

Thomas, M.K., Rastalsky, N., Lee, J.H., and Habener, J.F. (2000). Hedgehog signaling regulation of insulin production by pancreatic beta-cells. Diabetes *49*, 2039–2047.

Tseng, Y.H., Kokkotou, E., Schulz, T.J., Huang, T.L., Winnay, J.N., Taniguchi, C.M., Tran, T.T., Suzuki, R., Espinoza, D.O., Yamamoto, Y., et al. (2008). New role of bone morphogenetic protein 7 in brown adipogenesis and energy expenditure. Nature *454*, 1000–1004.

van Marken Lichtenbelt, W.D., Vanhommerig, J.W., Smulders, N.M., Drossaerts, J.M., Kemerink, G.J., Bouvy, N.D., Schrauwen, P., and Teule, G.J. (2009). Cold-activated brown adipose tissue in healthy men. N. Engl. J. Med. *360*, 1500–1508.

Virtanen, K.A., Lidell, M.E., Orava, J., Heglind, M., Westergren, R., Niemi, T., Taittonen, M., Laine, J., Savisto, N.J., Enerback, S., et al. (2009). Functional brown adipose tissue in healthy adults. N. Engl. J. Med. *360*, 1518–1525.

WHO (2009). Global Strategy on Diet (Physical Activity and Health).

Wu, X., Ding, S., Ding, Q., Gray, N.S., and Schultz, P.G. (2002). A small molecule with osteogenesis-inducing activity in multipotent mesenchymal progenitor cells. J. Am. Chem. Soc. *124*, 14520–14521.

Yan, Z., Cui, K., Murray, D.M., Ling, C., Xue, Y., Gerstein, A., Parsons, R., Zhao, K., and Wang, W. (2005). PBAF chromatin-remodeling complex requires a novel specificity subunit, BAF200, to regulate expression of selective interferon-responsive genes. Genes Dev. *19*, 1662–1667.

Yu, C., Markan, K., Temple, K.A., Deplewski, D., Brady, M.J., and Cohen, R.N. (2005). The nuclear receptor corepressors NCoR and SMRT decrease peroxisome proliferator-activated receptor gamma transcriptional activity and repress 3T3-L1 adipogenesis. J. Biol. Chem. *280*, 13600–13605.

Zehentner, B.K., Leser, U., and Burtscher, H. (2000). BMP-2 and sonic hedgehog have contrary effects on adipocyte-like differentiation of C3H10T1/2 cells. DNA Cell Biol. *19*, 275–281.

Zhang, J., Xia, W.L., and Ahmad, F. (1995). Regulation of pyruvate carboxylase in 3T3-L1 cells. Biochem. J. *306*, 205–210.

Zhang, Y., Proenca, R., Maffei, M., Barone, M., Leopold, L., and Friedman, J.M. (1994). Positional cloning of the mouse obese gene and its human homologue. Nature *372*, 425–432.

Zingaretti, M.C., Crosta, F., Vitali, A., Guerrieri, M., Frontini, A., Cannon, B., Nedergaard, J., and Cinti, S. (2009). The presence of UCP1 demonstrates that metabolically active adipose tissue in the neck of adult humans truly represents brown adipose tissue. FASEB J. *23*, 3113–3120.